DØ Note 5950-CONF

# Spin correlations in $t\bar{t}$ production in dilepton final states

The DØ Collaboration
*URL http://www-d0.fnal.gov*
(Dated: July 13, 2009)

A measurement of the correlation between the spin of the top and the spin of the anti-top quark produced in proton anti-proton scattering at a center of mass energy of $\sqrt{s} = 1.96$ TeV is presented using a double differential angular distribution. Final states with two electrons, two muons and one electron and one muon, missing transverse energy and at least two jets are analyzed. Data of an integrated luminosity of up to 4.2 fb$^{-1}$ taken with the DØ detector at the Tevatron collider are analyzed. We measure the correlation coefficient $C = -0.17^{+0.64}_{-0.53}$ (stat + syst).

*Preliminary Results for Summer 2009 Conferences*

## I. INTRODUCTION

Top quark physics plays an important role in testing the Standard Model (SM) and its possible extensions. One of the most important properties of the top quark, the spin, has not been carefully explored.

While the top quarks and antiquarks produced at hadron colliders are unpolarized, their spins are correlated [1]. Since at the Tevatron top pair production is dominated by $q\bar{q}$ scattering, a different spin correlation is analyzed compared to the LHC where top pair production is dominated by $gg$ scattering. The SM predicts that the top quark decays before its spin flips [2], in contrast with the lighter quarks, which are depolarized by QCD interactions long before they fragment [3]. The spin of the top quark is therefore reflected by its decay products. In this analysis it is assumed that top quarks decay exactly as predicted by the SM. Then the charged lepton from a leptonic top quark decay has a spin analyzing power of 1 at the tree level [4]. Therefore, the dilepton final states have the highest sensitivity to measure the correlation between the spins of pair-produced top and anti-top quarks [4, 5].

The observation of spin correlations would result in an upper limit on the lifetime of the top quark. This can be translated into a lower limit on the Kobayashi-Maskawa matrix element $|V_{tb}|^2$ without making assumptions about the number of quark generations [6]. Moreover, many scenarios beyond the SM [2, 7–11] predict different production and decay dynamics of the top quark, which could affect the observed spin correlation.

The only measurement of spin correlations between top and anti-top quarks so far was performed by the DØ Collaboration using an integrated luminosity of approximately 125 pb$^{-1}$ of $p\bar{p}$ collisions at $\sqrt{s} = 1.8$ TeV during Run I of the Tevatron collider [12]. The 68% confidence level given on a correlation coefficient was in agreement with the SM prediction. However, since the sample used for the measurement contained only six events, the sensitivity was too low to distinguish between a hypothesis of no correlation between the spins of top and antitop quarks and the correlation predicted by the SM.

Here, the same double differential angular distribution is used. For this measurement, we analyze the dileptonic decay channels where the $W$ bosons from the top and antitop quark decay into an electron and an electron neutrino or into a muon and a muon neutrino. The $ee$ channel with 1.1 fb$^{-1}$, the $e\mu$ channel with 4.2 fb$^{-1}$ and the $\mu\mu$ channel with 1.1 fb$^{-1}$ of integrated luminosity are analyzed separately and are then combined. The DØ detector is described in Ref. [13].

## II. OBSERVABLES

The $t$ and $\bar{t}$ are expected to be unpolarized, but to be correlated in their spins. Since top quarks decay before hadronizing, their spins at production are transmitted to their decay-daughter particles. The spin correlation is studied by analyzing the joint decay angular distribution of one $t$ daughter and one $\bar{t}$ daughter.

### A. Angular distributions

Hadronic top quark pair production and decay are known at NLO QCD with the spin of the top and antitop quarks taken into account [5]. The differential cross sections to order $\alpha_S^3$ are calculated, describing the $t\bar{t} + X$ production in a general spin configuration. The double differential distribution for a measurement of spin correlations between $t$ and $\bar{t}$ can be taken as:

$$\frac{1}{\sigma}\frac{d\sigma}{d\cos\theta_1 d\cos\theta_2} = \frac{1}{4}(1 - C\cos\theta_1\cos\theta_2) \ , \tag{1}$$

where $\sigma$ denotes the cross section of the channel under consideration and $C$ is a free parameter between -1 and 1 that depends on the choice of the spin basis. At tree level in the SM, where the spin analyzing power of the charged leptons is +1, $C$ represents the number of events where the $t$ and $\bar{t}$ spins are parallel minus the number of events where they are anti-parallel normalized by the total number of events. $\theta_1$ ($\theta_2$) describes the angle between the direction of flight of the lepton $\ell^+$ ($\ell'^-$) in the $t$ ($\bar{t}$) rest frame and a reference direction $\hat{\mathbf{a}}$ ($\hat{\mathbf{b}}$). The choice of spin basis determines the extent to which the spins of the top quarks are correlated. For the Tevatron it has been shown in [5] that an almost optimal choice for the spin basis is given by the beam basis

$$\hat{\mathbf{a}} = \hat{\mathbf{b}} = \hat{\mathbf{p}} \tag{2}$$

where $\hat{\mathbf{p}}$ is the direction of flight of one of the colliding hadrons in the $t\bar{t}$ rest frame.

In the absence of modifications due to selection efficiencies and acceptances, the spin correlation coefficient can be computed in terms of its expectation value

$$C = -9\langle \cos\theta_1 \cos\theta_2 \rangle \ , \tag{3}$$

The numerical value for the coefficient $C$, taking the beam axis as spin quantization axis, is given in Table 1.

| coefficient | LO | NLO |
|---|---|---|
| $C$ | 0.928 | 0.777 |

TABLE 1: LO and NLO results [5] for the spin correlation coefficient $C$ of the distribution (1) in the beam basis for $p\bar{p}$ collisions at $\sqrt{s} = 1.96$ TeV for the dilepton $t\bar{t}$ decay mode. The PDF CTEQ6L (LO) and CTEQ6.1M (NLO) were used, and the factorization and renormalization scale were both set equal to the top mass.

Templates for the distribution (1) are generated for different values of $C$ using a reweighting technique described in Section IV. They are compared to the data using a Maximum Likelihood fit to extract the coefficient $C$.

### B. Experimental measurement

The experimental measurement of the distribution (1) is performed as follows:

1. Reconstruct the top and anti-top momenta in the laboratory frame which is the rest frame of the colliding hadrons.
2. Perform a rotation-free boost from the laboratory frame to the $t\bar{t}$ rest frame. Define $\hat{\mathbf{a}}$ and $\hat{\mathbf{b}}$ in that frame.
3. Perform rotation-free boosts from the $t\bar{t}$ rest frame to the $t$ and $\bar{t}$ quark rest frames. Compute the direction $\hat{\mathbf{q_1}}$ ($\hat{\mathbf{q_2}}$) of the $t$ ($\bar{t}$) decay product $\ell^+$ ($\ell'^-$) in the $t$ ($\bar{t}$) rest frame.
4. Finally, compute $\cos\theta_1 = \hat{\mathbf{a}} \cdot \hat{\mathbf{q_1}}$, $\cos\theta_2 = \hat{\mathbf{b}} \cdot \hat{\mathbf{q_2}}$.

## III. EVENT SELECTION

The selections for the Run IIa $ee$, $e\mu$ and $\mu\mu$ channels are described in [14]. We use identical event samples as for the top mass measurement in the dilepton channels using the neutrino weighting method [15]. The selection in the $e\mu$ channel for Run IIb data is identical to that described in [16].

In the following we give a description of the selections. The only difference from the cross section analysis is that for the simulation of the $t\bar{t}$ signal we use the PYTHIA [17] event generator instead of ALPGEN [18]+PYTHIA, since ALPGEN does not generate top quark pairs without spin correlation. In PYTHIA we generate both spin correlated and uncorrelated samples with a reweighting technique described in Section IV.

### A. Lepton and Jet identification

The electrons used in the analysis are defined as clusters of calorimeter cells for which (a) the fraction of energy deposited in the electromagnetic section of the calorimeter has to be at least 90% of the total cluster energy, (b) the energy is concentrated in a narrow cone and isolated from further calorimeter energy, (c) the shape of the shower is compatible with that of an electron, (d) the electron matches a charged track in the tracking system. In order to further remove background we use (e) a likelihood discriminant that selects prompt isolated electrons based on the tracking system and calorimeter information. Both central ($|\eta| < 1.1$) and forward ($1.5 < |\eta| < 2.5$) electron candidates are used. Electrons that fulfill criteria (a) to (d) are referred to as "loose" electrons while those fulfilling criteria (a) to (e) are referred to as "tight" electrons.

The muons are defined using tracks reconstructed in the three layers of the muon system, with a matching track in the tracking system.

To further remove background, the sum of the charged track momenta in a cone of size $R = 0.5$ around the muon track must be smaller than 15% of the muon $p_T$. We also require muons to have the sum of calorimeter cell energies in an annulus with radius in the range $0.1 < \Delta\mathcal{R} < 0.4$ around the matched track to be less than 15% of the muon $p_T$.

Prompt muons are further selected by requiring that the distance of closest approach of the muon track with respect to the primary vertex is smaller than 0.2 cm for a muon track without a hit in the inner silicon tracking detector (SMT) and smaller than 0.02 cm for a muon track with a hit in the SMT.

Jets are reconstructed with a fixed cone algorithm [19] with radius $\mathcal{R} = \sqrt{(\Delta y)^2 + (\Delta\phi)^2} = 0.5$ where $y$ is the rapidity. Jet energies are corrected for the calorimeter response, additional energy from noise, pileup and multiple $p\bar{p}$ interactions in the same bunch crossing, and instrumental out-of-cone showering. In Run IIb jets are required to have at least two tracks originating from the primary vertex. For all the different channels, we require at least two jets, while the kinematic reconstruction only makes use of the two leading jets. $\not\!\!E_T$ is defined as equal in magnitude and opposite in direction to the vector sum of all significant calorimeter cell transverse energies corrected for the transverse energy of isolated muons and corrections to electron and jet energies. A more detailed description of the object reconstruction can be found in [20].

Sources of background are given by the production of electroweak bosons decaying into charged leptons. In the $ee$, $e\mu$ and $\mu\mu$ channels the dominating backgrounds come from $Z/\gamma^* \to e^+e^-$, $Z/\gamma^* \to \tau^+\tau^- \to \bar{\nu}_\tau\ell^+\nu_\ell\nu_\tau\ell^-\bar{\nu}_\ell$ with $\ell^\pm = e^\pm$ or $\mu^\pm$ and $Z/\gamma^* \to \mu^+\mu^-$ as well as diboson production ($WW, WZ$ and $ZZ$) when the boson decays lead to two charged leptons in the final state. Further background results from jets faking electrons, muons from semileptonic $b$ quark decay or from in-flight pion or kaon decay in a jet and large misreconstructed $\not\!\!E_T$.

### B. Selections

The event selection for each channel is optimized to minimize the expected statistical uncertainty on the cross section. To select top pair events one requires two isolated, oppositely charged, leptons for the $ee$, $\mu\mu$ and $e\mu$ channels. In Run IIa at least one jet is required to have $p_T > 30$ GeV and all other jets must have $p_T > 20$ GeV. In Run IIb the cut for the leading jet was lowered to 20 GeV. Jets are accepted in the region $|\eta| < 2.5$. Leptons are required to have $p_T > 15$ GeV in the $ee$, $\mu\mu$, $e\mu$ channels. Muons are accepted in the region $|\eta| < 2.0$, while electrons must be within $|\eta| < 1.1$ or $1.5 < |\eta| < 2.5$.

The selection on $\not\!\!E_T$ is crucial to reduce the otherwise large background from $Z/\gamma^* \to \ell^+\ell^-$. This background is particularly important in the $ee$ and $\mu\mu$ channels. Due to different resolutions in electron energies and muon momenta, the optimization of the selection leads to different selections in the three channels. In the $ee$ channel events with a dielectron invariant mass of $M_{ee} < 15$ GeV or $84 < M_{ee} < 100$ GeV are rejected. They are required to have $\not\!\!E_T > 35$ GeV ($\not\!\!E_T > 45$ GeV) for $M_{ee} > 100$ GeV ($15 < M_{ee} < 84$ GeV). The final selection in the $e\mu$ channel requires that $H_T$ (defined as the scalar sum of the leading lepton $p_T$ and the $p_T$ of the two most energetic jets) be greater than 115 GeV in Run IIa and greater than 105 GeV in Run IIb. This requirement allows rejection of the largest backgrounds for this final state arising from $Z/\gamma^* \to \tau^+\tau^-$ and diboson production. In the $\mu\mu$ channel events are required to have $\not\!\!E_T > 40$ GeV. To further reject $Z/\gamma^*$ background in the $\mu\mu$ channel, we require the significance of $\not\!\!E_T$ to exceed five standard deviations.

### C. Signal and background processes

Signal acceptances and efficiencies are derived from a combination of Monte Carlo (MC) simulation and data. Top quark pair production at $\sqrt{s} = 1.96$ TeV is simulated using the PYTHIA [17] generator assuming a top mass $m_{top}$ of 175 GeV. For cross checks we also use the ALPGEN [18] matrix element generator. These events are processed through PYTHIA [17] to simulate fragmentation, hadronization and decays of short-lived particles. The resulting events are processed through a full detector simulation using GEANT [21]. Each MC event is overlaid with a data event from a random bunch crossing to model the effects from detector noise and additional $p\bar{p}$ interactions. The same reconstruction process is then applied to both data and MC events to determine the cut efficiencies. Lepton trigger and identification efficiencies as well as lepton momentum resolutions are derived from $Z/\gamma^* \to \ell^+\ell^-$ data using a tag and probe method. The jet reconstruction efficiency and the jet resolution are adjusted to their measured values in data, and the missing transverse energy $\not\!\!E_T$ is recalculated accordingly.

Backgrounds are determined from a combination of MC simulation and data. The selection efficiencies for the $Z/\gamma^*$ background is estimated using MC samples generated by ALPGEN interfaced with PYTHIA while for diboson production they are estimated using PYTHIA. The $Z/\gamma^*$ and diboson processes are generated at leading order (LO) and are normalized to the next-to-next-to-leading order (NNLO) inclusive cross section for $Z/\gamma^*$ events and to the next-to-leading order (NLO) inclusive cross sections for diboson events [22, 23]. As the $Z$ boson $p_T$ is not properly described in the ALPGEN simulation, a $Z$ boson $p_T$ distribution reweighting has been performed for different jet multiplicity bins using $Z \to e^+e^-$ data events.

There are two kinds of instrumental background which are estimated from data. Fake electrons can arise from jets comprised of a leading $\pi^0/\eta$ and an overlapping or conversion-produced track. In the $ee$ and $e\mu$ channels the amount of fake electron background is fitted to the observed distribution of electron likelihood discriminant in the data as done in [20]. The shape of the electron likelihood is determined for real electrons in a pure $Z/\gamma^*$ data sample. The shape of the electron likelihood of fake electron background is then determined using a sample dominated by fake electrons. An isolated muon can be faked by a muon produced in a jet and the jet is not reconstructed. We measure the fraction $f_\mu$ of muons that appear isolated in a dimuon control sample dominated by fake isolated muons. In the $\mu\mu$ channel the number of events with a fake isolated muon contributing to the final sample is evaluated using the *matrix method* [20]. In the $e\mu$ channel the contribution from events with a real electron and a fake isolated muon is given by the number of events in a sample with no muon isolation requirement, where the electron and the muon have the same sign, multiplied by the fake rate $f_\mu$ measured as described above. Although they do not include high $p_T$ neutrinos, the processes $Z/\gamma^* \to \ell^+\ell^-$ might have a significant amount of $\not\!\!E_T$ due to mismeasurements or limited $\not\!\!E_T$ resolution. The $\not\!\!E_T$ spectra from pure $Z/\gamma^* \to \ell^+\ell^-$ data samples and MC agree well once the jet, electron, muon, and scalar $E_T$ resolutions of the MC have been adjusted to match the measured resolutions in the data. Thus in the $ee$ and $\mu\mu$ channel the expected contribution of $Z/\gamma^*$ background in the final sample is derived from MC.

### D. Event yields

In Tables 2–4 the expected number of background and signal events and the observed number of data events are summarized for all channels.

TABLE 2: Expected event yields by source for the $ee$ channel.

| | $t\bar{t} \to$ ee | $Z \to$ ee | $Z \to \tau\tau$ | Diboson | fake | Total | Data |
|---|---|---|---|---|---|---|---|
| Run IIa | $11.5 \pm 1.4$ | $1.3 \pm 0.3$ | $1.0 \pm 0.2$ | $0.5 \pm 0.2$ | $0.6 \pm 0.2$ | $14.8 \pm 1.5$ | 17 |

TABLE 3: Expected event yields by source for the $e\mu$ channel. In Run IIa the fake background is given for the sum of fake $e$ and $\mu$.

| | $t\bar{t} \to e\mu$ | $Z \to \tau\tau$ | Diboson | fake e | fake mu | Total | Data |
|---|---|---|---|---|---|---|---|
| Run IIa | $36.7 \pm 2.4$ | $4.5 \pm 0.7$ | $1.7 \pm 0.7$ | $2.6 \pm 0.6$ | | $45.5 \pm 2.7$ | 39 |
| Run IIb | $103.30 \pm 0.89$ | $4.57 \pm 0.85$ | $5.46 \pm 0.49$ | $3.0 \pm 1.3$ | $2.42 \pm 0.22$ | $118.75 \pm 1.9$ | 129 |

TABLE 4: Expected event yields by source for the $\mu\mu$ channel.

| | $t\bar{t} \to \mu\mu$ | $Z \to \mu\mu$ | $Z \to \tau\tau$ | Diboson | fake | Total | Data |
|---|---|---|---|---|---|---|---|
| Run IIa | $8.3 \pm 0.5$ | $3.3 \pm 0.3$ | $1.2 \pm 0.2$ | $0.7 \pm 0.1$ | $0.2 \pm 0.2$ | $13.6 \pm 0.7$ | 13 |

## IV. SIGNAL MODELING BY REWEIGHTING

For the measurement of $C$ as defined in Eqn. (1) $t\bar{t}$ samples with different values for the strength of the spin correlation $C$ have to be produced. PYTHIA is used for the generation. However, PYTHIA does not contain spin correlations between the top quarks. To introduce non-vanishing spin correlations each event has to be reweighted at the parton level by

$$w_r(\cos\theta_1 \cos\theta_2) = \frac{1}{4}(1 - C \cdot \cos\theta_1 \cos\theta_2) \ . \tag{4}$$

Figure 1 shows the distribution $\cos\theta_1 \cos\theta_2$ for the unreweighted $t\bar{t}$ sample ($C = 0$) (black) and the $t\bar{t}$ sample reweighted to the NLO QCD correlation value ($C = 0.777$) (red). A non-vanishing spin correlation leads to an asymmetry in the distribution. It has been checked that the selection cuts described in Section III do not introduce an asymmetry.

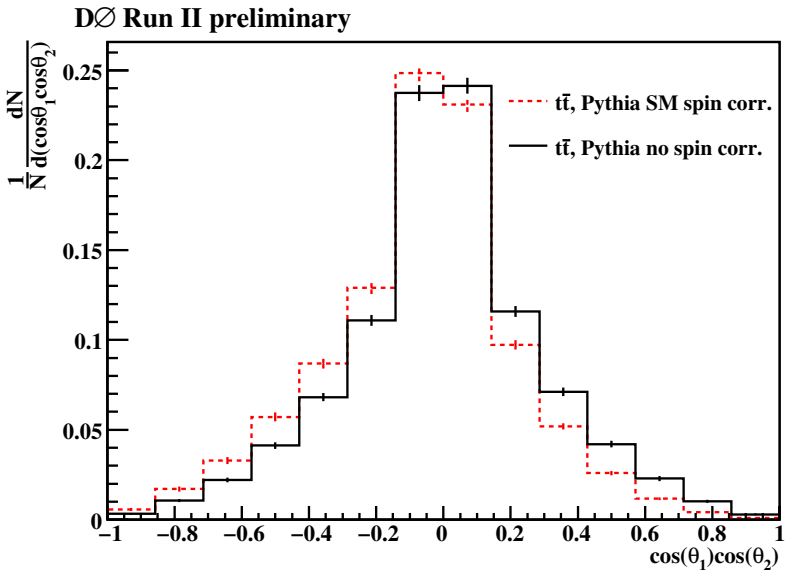


FIG. 1: The distribution $\cos\theta_1 \cos\theta_2$ for a $t\bar{t}$ sample including NLO QCD spin correlation (red dashed) and without spin correlation (black solid) for generated partons using PYTHIA.

## V. EVENT RECONSTRUCTION

The calculation of the angular correlation as described in Section II B requires boosts to the $t$ and $\bar{t}$ quark rest frames. Therefore every event has to be reconstructed. This is performed using the Neutrino Weighting Method as used for top quark mass measurements in the dilepton channel [15]. The only difference is that instead of calculating a weight distribution as a function of the top quark mass hypothesis, here a weight distribution as a function of $\cos\theta_1 \cos\theta_2$ is calculated.

In the dilepton final state, the momenta of the two charged leptons, two neutrinos and two $b$ quark jets are given by 18 kinematic quantities. We directly measure only 12 from the observed leptons and jets. Four additional constraints are provided by requiring two lepton-neutrino combinations to give the $W$ boson mass, and two $W$ boson + $b$-jet combinations to give the top mass (which we assume to be 175 GeV for top and antitop quark). Two quantities remain to be specified to allow solution of the kinematics.

### A. Neutrino Weighting

To obtain the two missing kinematic quantities, we take the neutrino pseudorapidities $\eta_1$ and $\eta_2$ from MC distributions. These $\eta$ distributions are well characterized by Gaussians with zero mean and unit width, and are found to be independent of top spin correlations. For each event, we pick ten values of $\eta_1$ and ten values of $\eta_2$, chosen in steps of equal probability so as to favor the more probable values. With each such choice, the kinematics of the event can be solved, with up to two solutions for each of the neutrino transverse momenta.

So far the information from the missing transverse energy inferred from the measured momenta in the event has not been used. This information is used to assign a weight to each of the solutions, for each set of assumed $\eta$s. For a given $\eta_1$ and $\eta_2$ we can calculate the missing transverse energy in the event under this assumption and compare it to the missing transverse energy actually measured. The weight distribution for each event is then calculated as

$$w = \sum_{\eta_1,\eta_2} \sum_{solutions} \exp\left(-\frac{\left(\not\!\!E_x{}^{calc} - \not\!\!E_x\right)^2}{2\sigma_{\not\!\!E_T}}\right) \exp\left(-\frac{\left(\not\!\!E_y{}^{calc} - \not\!\!E_y\right)^2}{2\sigma_{\not\!\!E_T}}\right)$$

where $\sigma_{\not\!\!E_T}$ is the resolution of the $x$ or $y$ component of missing transverse energy [15]. The resolution is the same

for the $x$ and $y$ direction. This assigns a high weight to assumed $\eta$s which are compatible with the observed missing energy.

A further complication arises due to the fact that it is not possible to tell which of the jets and leptons in the event came from the same top quark. Therefore all combinations are tried. This increases the possible number of solutions per event from four to eight.

### B. Resolution Sampling

The description of the weight calculation for a given event accounts for the detector resolution of the $\not\!\!E_T$ measurement, but it ignores the fact that jet and lepton energies may also be mismeasured. As a result, some configurations are either not solvable at reconstruction level or produce a weight that is incorrectly estimated. While this does not cause a change in the properties of weight distributions averaged over many events, it can have marked results for single events. Detector resolutions are accommodated in the weight calculation in the following manner: for each configuration of each MC event, 150 cases are calculated in which all jets and leptons are independently fluctuated according to their known resolutions. The 150 different weights are summed, making the weight distribution smoother. This number was found to be sufficient to obtain stable and smooth weight curves as well as to give acceptable computation times. For data events, the number of smears is increased to 2000 to ensure that the result does not depend on fluctuations in the smearing.

The probabilities that our procedure finds a valid solution for $t\bar{t}$ and background events are shown in Table 5. Events with no solution are dropped from the analysis. Only three of the 198 data events have no solutions. In the subsequent analysis, each retained event is weighted equally.

TABLE 5: Efficiencies for the neutrino weighter to find a kinematic solution. The $Z \to \tau\tau$, $Z \to \mu\mu$ and $Z \to ee$ backgrounds are shown combined, as are the different fake backgrounds.

| | $t\bar{t}$ | $Z$ | Diboson | fake | Data |
|---|---|---|---|---|---|
| Run IIa $ee$ | 0.97 | 0.77 | 0.91 | 0.90 | 1.00 |
| Run IIa $e\mu$ | 0.97 | 0.89 | 0.95 | 0.92 | 0.97 |
| Run IIa $\mu\mu$ | 0.98 | 0.90 | 0.82 | 0.91 | 0.92 |
| Run IIb $e\mu$ | 0.98 | 0.94 | 0.92 | 0.83 | 0.99 |

In Fig. 2 the weight distribution of $\cos\theta_1 \cos\theta_2$ for one example MC event is shown. The true value of $\cos\theta_1 \cos\theta_2$ is indicated by the arrow.

## VI. TEMPLATES

The neutrino weighting algorithm produces a weight distribution for every event. The mean of the $\cos\theta_1 \cos\theta_2$ weight distribution, $\mu_\theta$, is used for generating templates. Figure 3 shows $\mu_\theta$ for background and $t\bar{t}$ signal with NLO QCD spin correlation. The open black histogram shows the prediction for $t\bar{t}$ signal without spin correlation.

As a test for the validity of the reweighting method, Fig. 4 shows the results for the PYTHIA event generator including spin correlations in LO QCD (reweighted using $C = 0.928$) (black solid) compared to the ALPGEN LO event generator (blue solid) which contains spin correlations. The agreement between PYTHIA and ALPGEN shows that the reweighting method works well.

Templates are formed from the sum of the $t\bar{t}$ signals with a range of $C$ values and backgrounds as a function of $\mu_\theta$. The data $\mu_\theta$ distributions (or MC ensembles) are compared with these templates to obtain the best fit value for $C$.

## VII. CALIBRATION AND EXPECTED STATISTICAL UNCERTAINTIES

To check that the method is unbiased and to account for the expected statistical uncertainty properly, 1000 MC ensembles for various values $C_{\rm true}$ are generated, fluctuating every bin of every contribution using Poisson statistics. For every ensemble a binned Maximum Likelihood method is used to extract the measured value $C_{\rm meas}$. This is done by calculating the predicted number of events in all four channels and performing a Maximum Likelihood fit to the number of observed events in data. In each channel we use a 14 bin distribution of $\mu_\theta$ over the range $[-1, 1]$.

Systematic uncertainties are accounted for in the fit by modeling each independent source of systematic uncertainty as a Gaussian probability density function, $\mathcal{G}(\nu; 0, \mathrm{SD})$, with zero mean and width corresponding to one standard

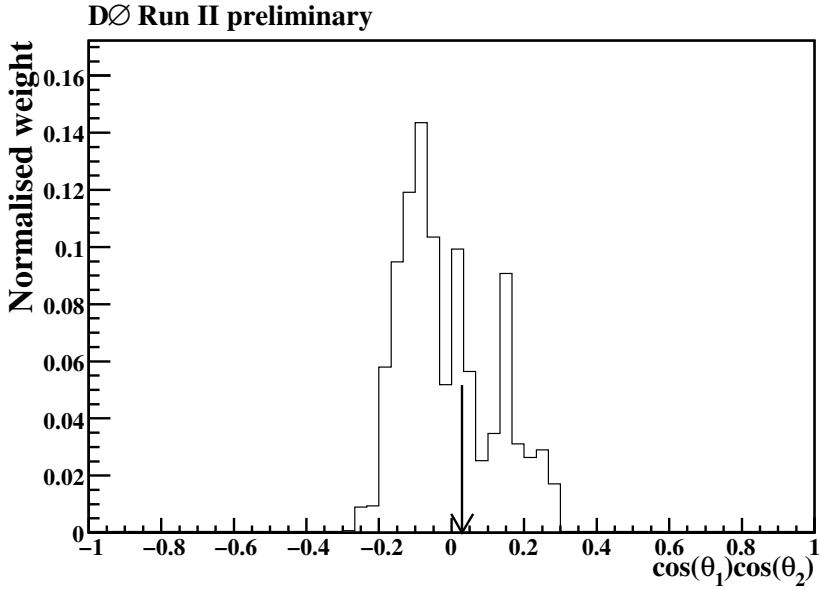


FIG. 2: Neutrino weight distribution for one fully reconstructed MC event. The true value of the quantity was calculated using the truth level neutrino and $t$ and $\bar{t}$ momenta and is marked with the arrow. The value of the mean of this distribution, $\mu_\theta$, used as estimator for the true value is: -0.01. Each weight distribution is normalized to unit area.

deviation (SD) of the parameter uncertainty. Correlations of systematic uncertainties between channels are naturally taken into account by using the same parameter for the same uncertainty source. The likelihood function

$$\mathcal{L} = \prod_{i=1}^{56} \mathcal{P}(n_i, m_i) \times \prod_{k=1}^{K} \mathcal{G}(\nu_k; 0, \mathrm{SD}_k)\,, \tag{5}$$

is maximized with $\mathcal{P}(n, m)$ representing the Poisson probability to observe $n$ events when $m$ events are expected. The product runs over the $4 \times 14 = 56$ bins. The $K$ independent sources of systematic uncertainty are taken into account by randomly choosing the nuisance parameters $\nu_k$ within the appropriate Gaussian distribution. The predicted number of events in each bin is the sum of the predicted number of background and expected $t\bar{t}$ events, which depends on $C$.

We have checked that this method delivers a correct treatment of bias, pull and statistical uncertainties by drawing events out of the MC pool to form ensembles instead of the per bin Poisson fluctuations of the discriminant as described above. The results of the two methods show good agreement.

## VIII. SYSTEMATIC UNCERTAINTIES

Systematic uncertainties are included by varying the template distributions and nuisance parameters incorporated into the maximum likelihood fit as described in Sect. VII.

The two main sources of systematic uncertainty are the variation of the top mass from 175 GeV to 170 GeV and the test of the reweighting method. We tested the latter by replacing the reweighted spin-correlated PYTHIA with ALPGEN and by replacing the spin-uncorrelated PYTHIA with MC@NLO [24], which also does not contain spin correlations, and observing the change in the measured $C$ parameter.

The statistical and systematic uncertainties on the measurement are listed in Table 6.

## IX. RESULT

A likelihood fit for data gives a measured value for the spin correlation parameter

$$C_{\mathrm{meas}} = -0.09^{+0.59}_{-0.58}\,(\mathrm{stat} + \mathrm{syst})\ . \tag{6}$$

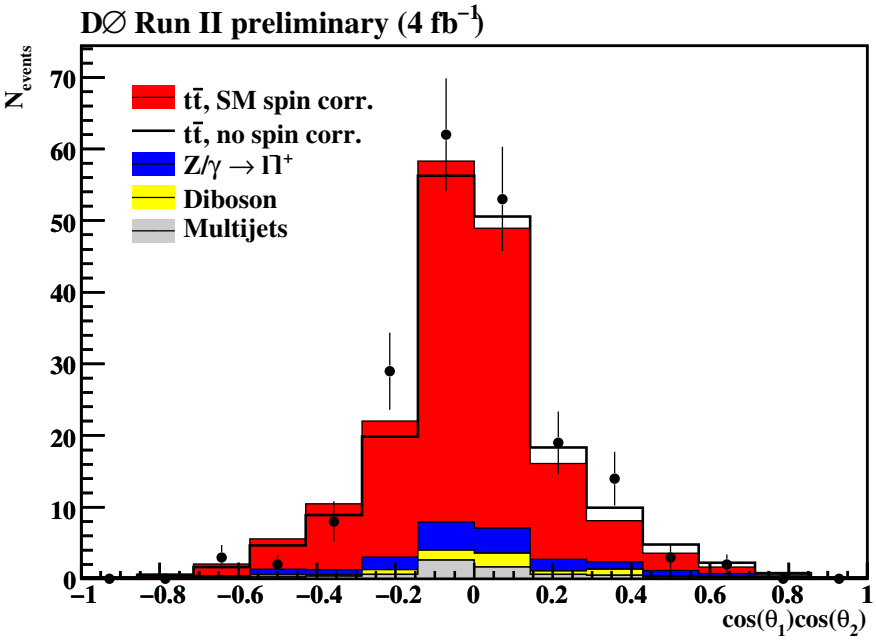


FIG. 3: The $\cos(\theta_1)\cos(\theta_2)$ distribution using the mean of the weight distribution per event for the full dilepton event sample. The sum of $t\bar{t}$ signal including NLO QCD spin correlation ($C = 0.777$) (red) and multijet (grey), diboson (yellow) and Drell-Yan (blue) background is compared to data. The open black histogram shows the prediction without $t\bar{t}$ spin correlation ($C = 0$).

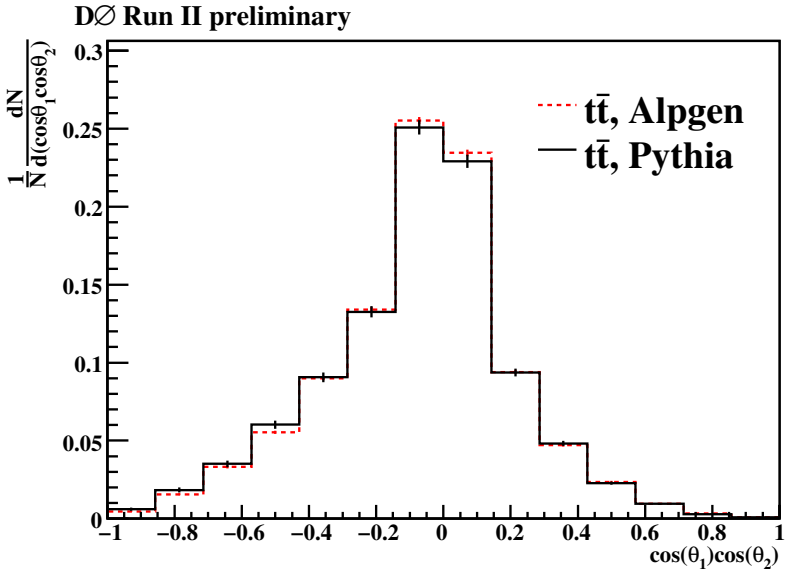


FIG. 4: The mean $\cos\theta_1 \cos\theta_2$ of the weight distribution. PYTHIA $t\bar{t}$ signal with $C = 0.928$ (black solid) is compared to ALPGEN $t\bar{t}$ signal (red dashed). The $e\mu$ channel in Run IIb is shown.

To obtain the expected result and uncertainty, MC ensembles are generated for various values of $C_{\rm true}$ including systematic uncertainties. Then the likelihood-ratio ordering principle is applied on the distributions of measured $C_{\rm meas}$ for each generated $C_{\rm true}$, according to the Feldman-Cousins procedure [25].

The calibrated result extracted from the Feldman-Cousins procedure is

$$C = -0.17^{+0.64}_{-0.53}\,(\text{stat} + \text{syst})\ . \tag{7}$$

The result is shown in Fig. 5. Although our result for value for C differs from that predicted in NLO QCD by nearly

TABLE 6: Summary of uncertainties on $C$.

| Source | $\Delta C$ |
|---|---|
| Statistical only | +0.503 -0.510 |
| Signal modeling ALPGEN | +0.197 -0.120 |
| Signal modeling MC@NLO | +0.107 -0.085 |
| Top Mass | +0.215 -0.223 |
| Jet energy scale | +0.012 -0.022 |
| Jet energy resolution | +0.000 -0.030 |
| Monte Carlo background x-section | +0.008 -0.008 |
| Monte Carlo signal & bkg branching ratio | +0.002 -0.002 |
| Monte Carlo bkg scale factors | +0.000 -0.000 |
| Monte Carlo statistics | +0.010 -0.010 |
| $t\bar{t}$ cross section error | +0.008 -0.005 |
| Luminosity | +0.002 -0.002 |
| Total systematic | +0.312 -0.270 |

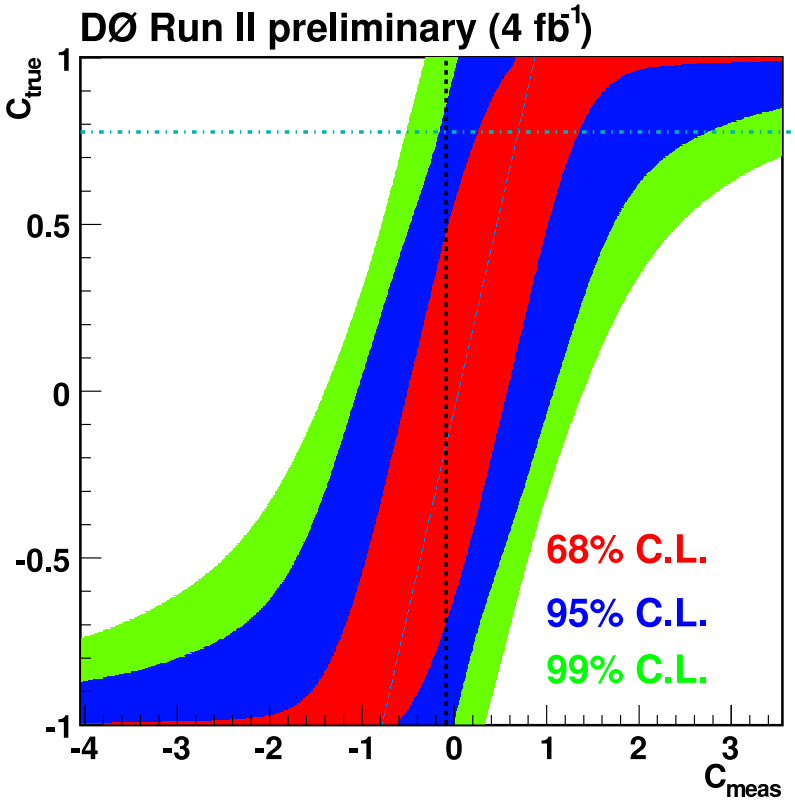


FIG. 5: The 68% (inner band), 95% (middle band), and 99% (outer band) C.L. band for $C_{\rm true}$ as a function of $C_{\rm meas}$. The thin blue line indicates the most probable value of $C_{\rm true}$ as a function of $C_{\rm meas}$ and represents therefore the bias of the method. The vertical black line depicts the measured value $C_{\rm meas} = -0.090$. The horizontal dash-dotted line indicates the NLO QCD value $C_{\rm true} = 0.777$. The combined result of the Run IIa $ee$, $e\mu$, $\mu\mu$ and the Run IIb $e\mu$ channels is shown.

2 SD, it is consistent with the SM.

## X. CONCLUSION

Spin correlations between top and antitop quarks in $t\bar{t}$ production have been measured using a double differential angular distribution. A correlation coefficient characterizing the degree of spin correlation of $C = -0.17^{+0.64}_{-0.53}$ has been measured. This agrees with the SM prediction for a spin 1/2 top quark of $C = 0.777$ in NLO QCD within 2 SD.


[1] V. D. Barger, J. Ohnemus and R. J. N. Phillips, Int. J. Mod. Phys. A **4**, 617 (1989).
[2] I. I. Y. Bigi, Y. L. Dokshitzer, V. A. Khoze, J. H. Kühn and P. M. Zerwas, Phys. Lett. B **181**, 157 (1986).
[3] A. F. Falk and M. E. Peskin, Phys. Rev. D **49**, 3320 (1994).
[4] A. Brandenburg, Z. G. Si and P. Uwer, Phys. Lett. B **539**, 235 (2002).
[5] W. Bernreuther, A. Brandenburg, Z. G. Si and P. Uwer, Nucl. Phys. B **690**, 81 (2004).
[6] T. Stelzer and S. Willenbrock, Phys. Lett. B **374**, 169 (1996).
[7] W. Bernreuther, M. Flesch and P. Haberl, Phys. Rev. D **58**, 114031 (1998).
[8] I. I. Y. Bigi, Phys. Lett. B **175**, 233 (1986).
[9] M. Jezabek and J. H. Kühn, Phys. Lett. B **329**, 317 (1994).
[10] G. R. Goldstein, K. Sliwa and R. H. Dalitz, Phys. Rev. D **47**, 967 (1993).
[11] W. Bernreuther, M. Fuecker and Y. Umeda, Phys. Lett. B **582**, 32 (2004).
[12] B. Abbott *et al.* [D0 Collaboration], Phys. Rev. Lett. **85**, 256 (2000).
[13] V. M. Abazov *et al.* [D0 Collaboration], Nucl. Instrum. Methods A **565**, 6463 (2006).
[14] V. M. Abazov *et al.* [D0 Collaboration], arXiv:0901.2137 [hep-ex].
[15] V. M. Abazov *et al.* [D0 Collaboration], arXiv:0904.3195 [hep-ex].
[16] The D0 Collaboration, DØ Note 5897-CONF.
[17] T. Sjöstrand *et al.*, Comp. Phys. Commun. **135**, 238 (2001).
[18] M. L. Mangano *et al.*, JHEP **0307**, 001 (2003).
[19] G.C. Blazey *et al.*, arXiv:hep-ex/0005012 (2000).
[20] V. M. Abazov *et al.* [D0 Collaboration], Phys. Rev. D **76**, 052006 (2007).
[21] R. Brun and F. Carminati, CERN Program Library Long Writeup W5013, 1993 (unpublished).
[22] J.M. Campbell and R.K. Ellis, Phys. Rev. D **60**, 113006 (1999).
[23] J.M. Campbell and R.K. Ellis, MCFM - Monte Carlo for FeMtobarn processes, http://mcfm.fnal.gov.
[24] S. Frixione and B. R. Webber, JHEP **0206**, 029 (2002).
[25] G. J. Feldman and R. D. Cousins, Phys. Rev. D **57**, 3873 (1998).